Mon. Not. R. Astron. Soc. **283,** 1311–1321 (1996)

Double-peaked Balmer line emission in the radio-quiet AGN RX J1042 + 1212

E. M. Puchnarewicz, K. O. Mason and F. J. Carrera★

Mullard Space Science Laboratory, University College London, Holmbury St. Mary, Dorking, Surrey RH5 6NT

Accepted 1996 August 5. Received 1996 August 2; in original form 1996 April 4

ABSTRACT

We present optical and X-ray spectra of a radio-quiet, X-ray-selected AGN, RX J1042 + 1212 ($z = 0.271$). The Hα and Hβ emission lines are very broad (with full widths at half maximum of ~ 10000 km s^{-1}) and have double-peaked profiles. Such features are rarely observed in AGN in general, but are even more unusual in radio-quiet objects. The analysis of the *ROSAT* PSPC data reveals a non-varying, unabsorbed spectrum with an energy spectral index $\alpha_x = 1.2$ and little or no emission from a soft X-ray excess. The slope of the optical spectrum is similar, $\alpha_{opt} = 1.0$, and is consistent with an extrapolation of the X-ray spectrum, suggesting that the same power-law continuum may dominate throughout, and that the big blue bump component is relatively weak.

We look for a link between these various properties, and investigate models of double-peaked Balmer line emission in AGN. An accretion disc origin is unlikely in RX J1042 + 1212, as this model predicts that lines emitted by a disc should have a net gravitational redshift (both Hα and Hβ have a net blueshift). Emission from two broad-line regions, each gravitationally bound to one component of a supermassive black hole binary, is a possibility if the two components are similar in size and nature. Alternatively, the lines (or at least the narrow peaks of the lines) may be produced by a double-sided jet or bipolar flow.

Key words: line: profiles – galaxies: active – galaxies: individual: RX J1042 + 1212 – galaxies: Seyfert – X-rays: galaxies.

1 INTRODUCTION

The structure and strength of the line emission in AGN reveals much about the nature of the central engine and the broad-line regions (BLRs). Double-peaked Balmer line profiles are rarely observed, but are of special interest because they place specific constraints on the geometry and motions of the gas. Their rarity is also intriguing; only ~25–30 AGN with double-peaked profiles have been observed and most of these (~80 per cent) are radio-loud, even though radio-loud objects make up only ~10 per cent of the overall AGN population. Any successful model of double-peaked line-emitting AGN must also explain why these objects prefer a radio-loud host.

Several models have been proposed as the origin of double-peaked lines, for example, the outer regions of an accretion disc (AD) (e.g. Collin-Souffrin et al. 1980; Alloin, Boisson & Pelat 1988; Pérez et al. 1988), from a binary BLR, i.e., two BLRs in orbit, each gravitationally bound to its own supermassive black hole (Begelman, Blandford & Rees 1980; Gaskell 1983, 1988; Stockton & Farnham 1991), or from a double-sided jet or cone (e.g. Zheng, Binette & Sulentic 1990; Veilleux & Zheng 1991; Zheng, Veilleux & Grandi 1991). For one model to be generic to all AGN it must accommodate the wide range of properties observed, which include both red- and blue-dominant peaks and profile and flux variability [including changes from red- to blue-dominant; see, e.g., Eracleous & Halpern (1994) for a sample of objects].

The AD is particularly attractive as it is already a popular model for the origin of the big blue bump (BBB; this component dominates the spectra of most radio-quiet AGN, it

★Present address: Instituto de Física de Cantabria CSIC-UC, Facultad de Ciencias, Avenida de los Castros, E.39005, Santander, Spain.

rises through the optical/UV, and the soft X-ray excess is believed to be its high-energy tail; see, e.g., Edelson & Malkan 1986; Walter & Fink 1993; Elvis et al. 1994). However, circular ADs cannot predict double-peaked line profiles with red-dominant peaks, although Eracleous et al. (1995) demonstrated that these problems, and others related to profile variability, could be overcome by invoking elliptical discs. All AD models, however, predict that the line will have a net gravitational redshift (Eracleous et al. 1995), yet some objects have lines which show a net blueshift, e.g., IC 4329A, Akn 120 and M81 (Marziani, Calvani & Sulentic 1992; Bower et al. 1996; see also Eracleous & Halpern 1994).

Binary BLRs have been proposed as the source of double-peaked emission in OX 169 (Stockton & Farnham 1991) and possibly in 3C 390.3 (Zheng et al. 1991). However, this model is not appropriate in all cases; for example, Halpern & Filippenko (1988) demonstrated that the positions of the lines in Arp 120 did not vary within the timescale predicted. Peterson et al. (1990) suggested that the profiles observed in NGC 5548 may be due to a combination of emission from both an AD *and* a binary BLR.

The double-sided jet model has the greatest degree of flexibility, due to the large number of free parameters in the model and the possibility of different conditions in the opposing jets, and was successfully used to fit the Hα profile of 3C 390.3 (Zheng et al. 1991). Also, Storchi-Bergmann, Baldwin & Wilson (1993) suggested that the recent appearance of a broad, double-peaked component in the LINER galaxy NGC 1097 (which is already known to contain four faint optical jets) may be due to a new jet in formation.

We present optical and X-ray data for a newly identified, X-ray-selected, radio-quiet AGN with double-peaked Balmer line emission. RX J1042 + 1212 is a $z = 0.271$ Seyfert 1 galaxy, which was discovered during the optical identification campaign of the *ROSAT* International X-ray and Optical Survey (RIXOS; Mason et al. 1996, in preparation). Its Hα and Hβ lines are strong and very broad (FWHM $\sim 10\,000$ km s^{-1}) and exhibit narrow peaks separated by ~ 3000 km s^{-1}. As a rare example of its kind, it presents a further opportunity to investigate the nature of double-peaked emission in radio-quiet AGN.

The optical and X-ray spectra of RX J1042 + 1212, including model fits to the soft X-ray data, are presented in Section 2. In Section 3, we parametrize the emission-line properties by fitting Gaussian components to the Hα and Hβ profiles. We also investigate the continuum overall, from the radio to X-rays, and compare these results and the emission line properties with those of other samples of AGN. Our interpretation of these results in the context of current models for double-peaked Balmer emission is discussed in Section 4.

2 OBSERVATIONS

2.1 Optical

RX J1042 + 1212 was observed on 1994 February 16 using the Faint Object Spectrograph (FOS) on the 2.9-m Isaac Newton Telescope at La Palma. The spectrum covers a range from 3500 to 10 000 Å, with a resolution of 15–20 Å FWHM in the red and 8–10 Å FWHM in the blue. It was taken with a narrow slit positioned at the parallactic angle, and the exposure time was 600 s.

The spectra were extracted and sky-subtracted using Mukai's (1990) implementation of Horne's (1986) optimal extraction algorithm. Wavelength calibrations were derived from Cu-Ar arc spectra, while observations of photometric

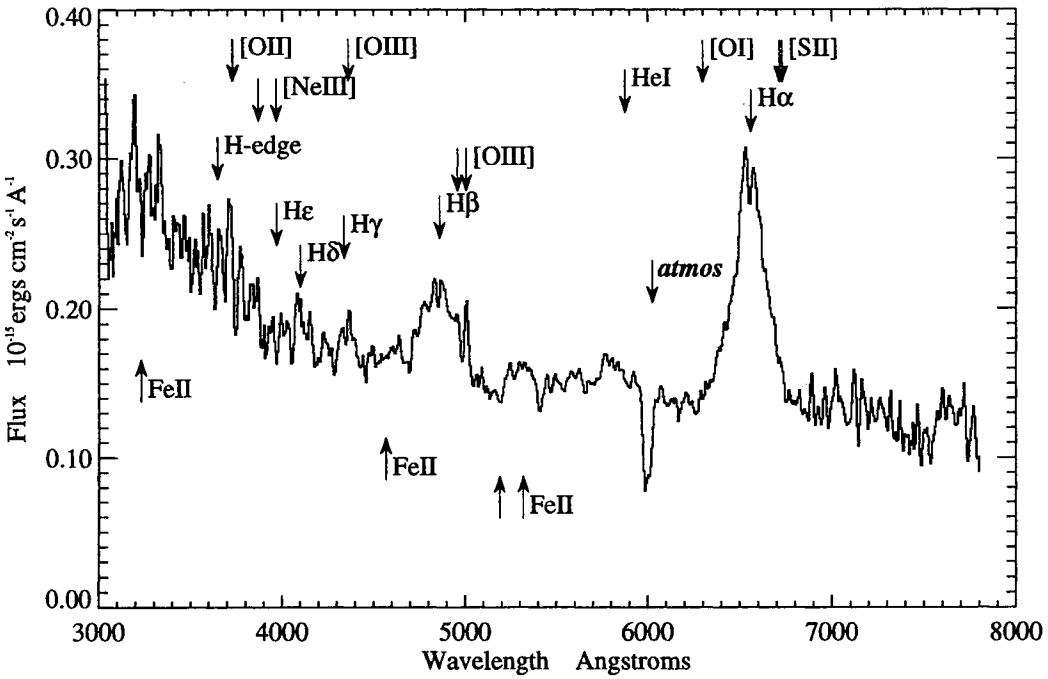

Figure 1. The optical spectrum of RX J1042 + 1212 taken at the INT in 1994 February. The spectrum has been smoothed using a boxcar filter with a width of three bins and has been redshifted into the rest-frame of the AGN ($z = 0.271$). The expected positions of lines commonly found in AGN spectra are indicated; the feature at ~ 6000 Å is caused by atmospheric extinction.

Table 1. X-ray and optical positions.

	RA (J2000.0)	Dec (J2000.0)	V magnitude	count rate count s^{-1}
Optical[1]	10 42 25.7	+12 12 40	18.4	
X-ray[2] (PSPC)	10 42 25.9	+12 12 46		$4.7\pm0.3 \times 10^{-2}$

[1]From Mason et al. (1996); the magnitude is measured from the optical spectrum and should be considered uncertain; the positional error is ± 1 arcsec.
[2]The count rate is measured over 0.1–2.0 keV, and the position is calculated from the centroid of the PSPC image; positional errors are a few arcseconds.

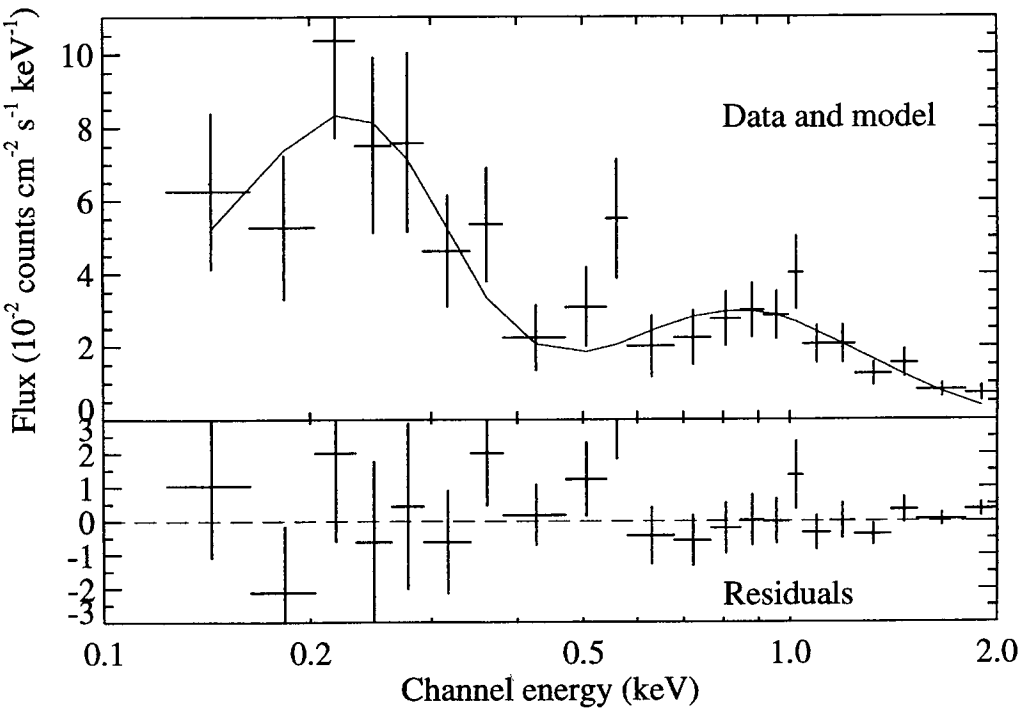

Figure 2. [top] The *ROSAT* PSPC spectrum of RX J1042 + 1212 with the best-fitting power-law model (thin line). [bottom] The residuals on the fit.

standards were used for flux calibration. The spectrum is shown in Fig. 1; the optical position and V magnitude are listed in Table 1.

2.2 Soft X-ray spectrum

2.2.1 Data

The soft X-ray spectrum of RX J1042 + 1212 was obtained on 1991 November 22 using the Position Sensitive Proportional Counter (PSPC; Pfefferman et al. 1986) on *ROSAT*; the exposure time was 10209 s. The PSPC has a 2° field of view and covers a range of 0.1–2.4 keV. Using the standard ASTERIX software, the source spectrum was extracted using a circle with radius 2.5 arcmin, and a source-free, annular region (with radii of 3.0 and 5.5 arcmin) surrounding the target was used for background subtraction. Counts were binned to yield at least 20 per energy bin, ignoring channels 1–11 and 201–256 where the response is uncertain. The spectrum has been corrected for all instrumental effects including vignetting, dead-time and particle contamination, and is illustrated in Fig. 2. The centroid of the X-ray emission, determined from the PSPC image, is consistent with the optical position; the soft X-ray count rate and position are listed in Table 1.

2.2.2 Model fitting

The reduced PSPC data were fitted using the XSPEC spectral fitting software. The Galactic column in the direction of the source, $N_{\rm HGal} = 2.8 \times 10^{20}$ cm^{-2}, was calculated by interpolating between the 21-cm measurements of Stark et al. (1992). A single power law with cold absorption provided a good fit to the data ($\chi^2_\nu = 0.9$; see Fig. 2), converging to an X-ray spectral energy index, α_x, of 1.0 ± 0.7 (errors are 90 per cent; α_x and all spectral indices are defined such that $F_\nu \propto \nu^{-\alpha}$) and a Galactic column of $2.1^{+2.2}_{-1.5} \times 10^{20}$ cm^{-2}. Confidence contours for the power-law model are shown in Fig. 3, and indicate that the data are consistent with little or no absorption intrinsic to the AGN (assuming, of course, that the power-law model is an accurate representation of the intrinsic spectrum).

If the absorbing column is fixed at the Galactic value, the best-fitting power-law index converges to $1.20^{+0.16}_{-0.17}$, with no significant change to χ^2_ν ($=0.9$; see Table 2 for details of all

the X-ray spectral fits). This model is similar to that used to fit the three-colour data in the original RIXOS survey, and gives a result which agrees within 90 per cent [i.e., $0.96^{+0.11}_{-0.11}$ (Mittaz et al. 1996, in preparation); both sets of errors are quoted to 90 per cent].

2.2.3 *Variability*

To check for X-ray variability, we divided the PSPC data into the individual observing intervals (OBIs; these comprised 10 periods of ~1000 s taken over two and a half days) and measured the count rate and spectrum for each. However, we could find no evidence for significant flux or spectral variability for the duration of the X-ray observation.

3 THE SPECTRUM OF RX J1042+1212

RX J1042+1212 was included in studies of the optical and X-ray properties of the RIXOS AGN (Puchnarewicz et al. 1996, hereafter P96; Puchnarewicz et al. 1997, in preparation), and was notable as an outlier from the anticorrelation between α_x and the Balmer line FWHM; indeed, RX J1042+1212 has the broadest Balmer emission of all AGN in the RIXOS sample. In the following analysis, we present an investigation of the emission-line and continuum properties of RX J1042+1212.

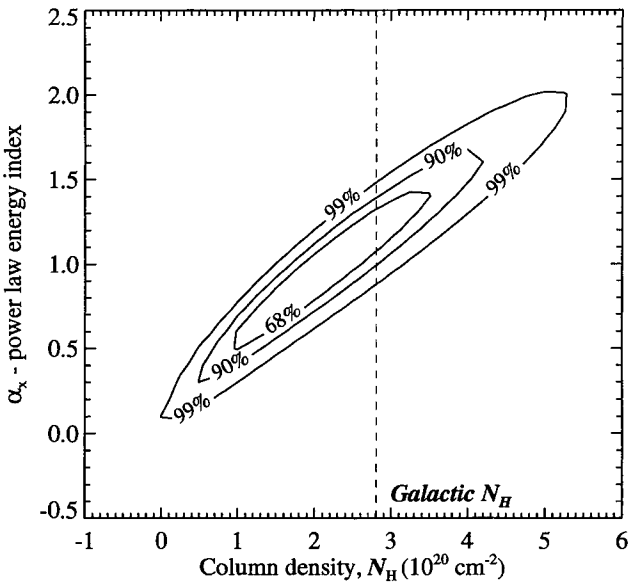

Figure 3. Confidence contours for the power-law model fit to RX J1042+1212. Also plotted as a thin, dashed line is the Galactic absorbing column density interpolated from the Stark et al. (1992) measurements.

3.1 Double-peaked Balmer lines

A closer examination of the optical spectrum (plotted in Fig. 1) reveals that both Hα and Hβ are double-peaked as well as being very broad (see also Figs 4–6). In order to model the complex shapes of the Balmer line profiles and to measure line fluxes and equivalent widths (EWs), we have fitted the data with combinations of Gaussians (using a second-order polynomial for the underlying continuum).

3.1.1 *Hα*

Initially, the Hα feature was fitted with a single component for the line emission and an 'absorption dip' (see Fig. 4a). The FWHM of the broad emission component is 8900 km s^{-1} (the FWHM in Tables 3 and 4 have been deconvolved from the instrumental profile which is ~800 km s^{-1}), and both the 'dip' and the line have a central wavelength of 6553 Å. A better representation of the data was obtained using a three-component fit, with a broad underlying component and separate red and blue peaks (Fig. 4b). For this model, the FWHM of the broad component is 10900 km s^{-1}, while the red and blue peaks are much narrower (1500 and 1400 km s^{-1} respectively). The blue peak is slightly stronger than the red, and the separation between the two is 2600 km s^{-1}.

The fits to Hα are illustrated in Fig. 4 and detailed in Table 3.

3.1.2 *Hβ*

Fitting the Hβ profile is less straightforward (see Fig. 5). It is likely to be blended with optical Fe II, as this is very strong elsewhere in this region (see the blends at 4570 and 5250 Å in Fig. 1). By fitting a single Gaussian to Hβ (and narrower components to [O III] $\lambda\lambda$4959, 5007; see Fig. 5a), we derive a FWHM (for Hβ) of 11300 km s^{-1}. We also tried adding an absorption dip in Hβ to this model (Fig. 5b), although this made little difference to the overall fits (which may be largely due to the relatively poor data quality around Hβ). Like Hα, the dip is slightly blueshifted with respect to [O III] $\lambda\lambda$4959, 5007. The [O III] $\lambda\lambda$4959, 5007 lines are unresolved, and their flux is low compared with Hα and Hβ. Parameters from these fits are given in Table 4.

Table 2. Results of single power-law fits to the PSPC spectrum.

Fit	Index α_x	Normalization keV cm^{-2} s^{-1} keV^{-1}	Galactic N_H (N_{HGal}) 10^{20} cm^{-2}	χ^2_ν/dof K
(1)	1.0±0.7	1.5±0.3 × 10^{-4}	$2.1^{+2.2}_{-1.5}$	17.9/19
(2)	$1.20^{+0.16}_{-0.17}$	1.6±0.2 × 10^{-4}	2.8 (fixed)	18.5/20

(1) Best-fitting power-law model with the Galactic column (N_{HGal}) free – errors are 90 per cent. (2) Best-fitting power-law model with N_{HGal} fixed at the Stark et al. (1992) value.

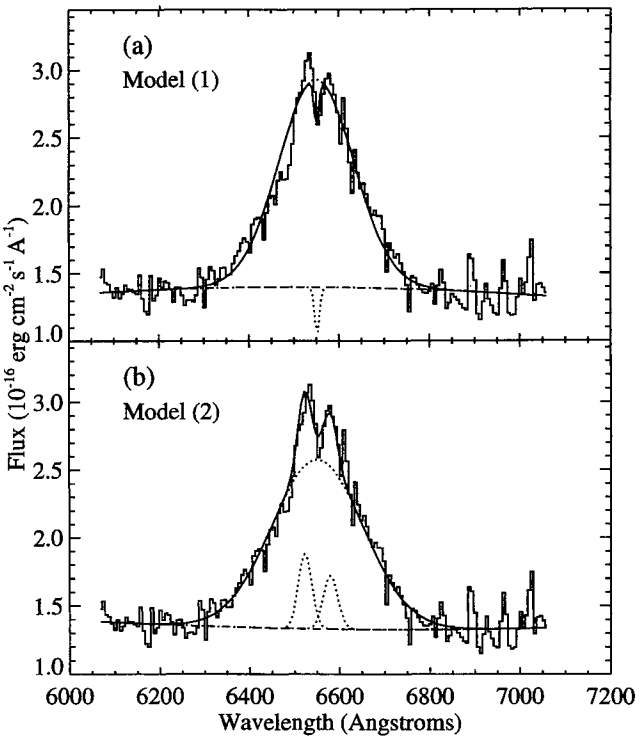

Figure 4. The profile of Hα (histogram) compared with multi-Gaussian fits to the data: (a) a broad emission feature plus an 'absorption dip' [model (1) from Table 3]; (b) a broad underlying component plus red and blue peaks [model (2) from Table 3]. The total fit is plotted as a solid line, the model fitted to the continuum as a dashed line and fits to the individual Gaussian components (plus the continuum) as dotted lines.

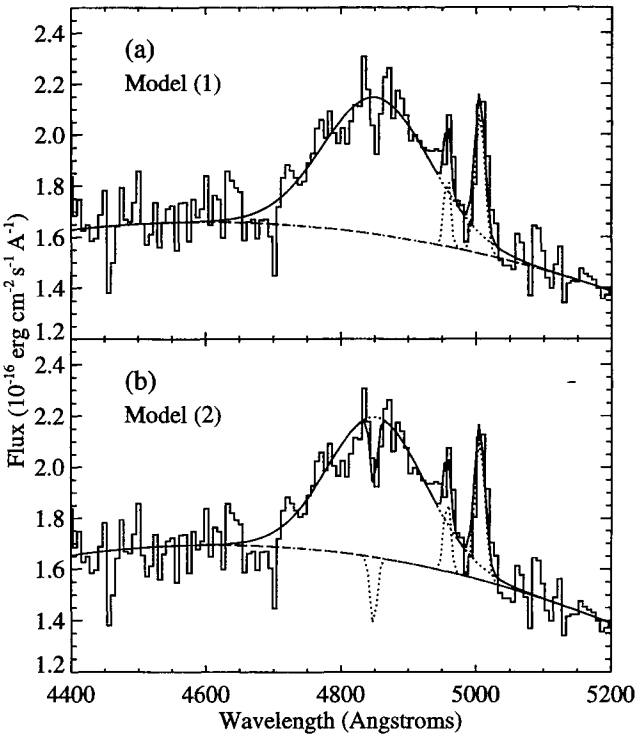

Figure 5. The profile of Hβ (histogram) compared with multi-Gaussian fits to the data: (a) a broad Hβ component plus narrower components for [O III] $\lambda\lambda$4959, 5007 [model (1) in Table 4]; (b) the same as (a) but with an additional 'absorption dip' in Hβ [model (2) in Table 4]. The total fit is plotted as a solid line, the model fitted to the continuum as a dashed line and fits to individual Gaussian components (plus the continuum) as dotted lines.

3.1.3 Balmer line profiles

In Fig. 6, we compare the profiles of Hα and Hβ directly. The fitted continuum [from model (2) in Table 3] has been subtracted from the region around Hα. For Hβ, the fitted continuum and fits to the [O III] $\lambda\lambda$4959, 5007 lines [using model (1) in Table 4] have been subtracted; then the remaining data have been multiplied by a factor of 2.8 to match the Hα peak. The profiles have a similar shape, and both display the double-peaked profile; the blue peak appears to be stronger than the red in Hα. The excess emission in the wings of Hβ relative to Hα (see Fig. 6) may be due to Fe II.

The centre of the 'red peak' of the Hα line is coincident with the expected position of [N II] λ6584; however, there are a number of reasons why we believe that this is not caused by [N II] λ6584 emission. First, despite the poorer signal in the Hβ region, the Hα and Hβ profiles show a remarkable similarity when plotted in velocity space (see Fig. 6); note in particular the relative positions of the peaks and the dip which are very closely matched. This is unlikely to be coincidental. Secondly, if the red peak was actually due to [N II] λ6584, this would imply (a) that the blue peak was a separate narrow component of Hα, blueshifted with respect to the other (forbidden) narrow lines by $\sim$1600 km s^{-1}; and (b) that there was no significant Hα emission from the narrow-line region (i.e., at 6562 Å), despite strong [N II] λ6584 emission at the systemic velocity (which in any case is generally very weak in luminous AGN like RX

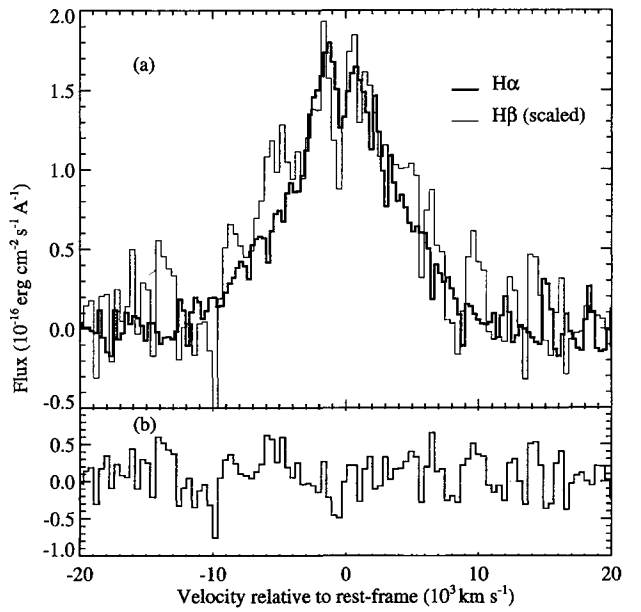

Figure 6. (a) A direct comparison of the Hα and Hβ line profiles. Hα is plotted as a thick histogram while Hβ is plotted as a thin histogram. For Hα, the fitted continuum from model (1) in Table 3 has been subtracted. For Hβ, the fits to the continuum and to the [O III] $\lambda\lambda$4959, 5007 lines using model (2) in Table 4 have been subtracted and the remaining data have then been multiplied by a factor of 2.8 to match the Hα profile. (b) The difference between the Hα and scaled Hβ profiles (i.e. Hβ – Hα).

Table 3. Measurements of the Hα parameters.

Model	Component	Position Å	FWHM km s^{-1}	Flux 10^{-14} erg cm^{-2} s^{-1}	EW Å
(1)	emission line	6553	8900	3.3	240
	absorption dip	6553	unresolved	–0.05	–3
(2)	broad	6553	10900	2.9	220
	blue peak	6526	1400	0.2	20
	red peak	6583	1500	0.2	10

(1) Two-component model with one Gaussian representing the Hα emission line and a second the 'absorption dip'. (2) Three-Gaussian model with a very broad underlying component and red and blue intermediate-width peaks. Measurements are taken from the spectrum shown in Fig. 1. The position is the central wavelength of the Gaussian component; the FWHM is calculated from the Gaussian σ and has been deconvolved from the instrumental profile. The flux and EW have been measured directly from the spectrum after the continuum and model flux from other fitted components have been subtracted.

Table 4. Measurements of Hβ and [O III] λλ4959, 5007 parameters.

Model	Component	Position Å	FWHM km s^{-1}	Flux 10^{-14} erg cm^{-2} s^{-1}	EW Å
(1)	Hβ	4854	11300	0.72	50
	[OIII]λ5007	5007	unresolved	0.08	6
	[OIII]λ4959	4959	unresolved	0.02	2
(2)	Hβ	4855	10400	0.67	40
	absorption dip	4851	unresolved	–0.04	1
	[OIII]λ5007	5007	unresolved	0.09	7
	[OIII]λ4959	4959	unresolved	0.03	2

(1) Three-component model with separate Gaussians representing the Hβ, [O III] λ5007 and [O III] λ4959 lines. (2) Four-component model with an additional 'absorption dip' in Hβ. Other details are the same as for Table 3.

J1042 + 1212). A physical interpretation of this would be difficult. Finally, the [O III] λ5007 line is unresolved; therefore one would also expect the same of any [N II] λ6584 emission, yet the red peak in Hα has been resolved.

The observed Hα/Hβ flux ratio is 5^{+1}_{-4} (these errors have been estimated by fitting the upper and lower limits on the Gaussian profiles by eye), and the ratio of their peaks is 2.8. Assuming that the intrinsic Hα/Hβ flux ratio is 2.8 (the appropriate value for case B recombination), there is no evidence for significant dust reddening in RX J1042 + 1212. In Section 2.2.2, we showed that there was no evidence either for intrinsic absorption in cold gas, for a single power-law model fit to the X-ray spectrum.

3.2 Multiwavelength continuum

The optical and X-ray spectra of RX J1042 + 1212 in the rest-frame of the AGN are plotted in Fig. 7. We have also searched in the radio and IR for any emission associated with this source; however, *no* 20-cm radio source was found stronger than 1.4 mJy within a few arcminutes of the optical position of RX J1042 + 1212 (J. J. Condon, private communication), neither are there any *IRAS* sources within a radius of 20 arcmin. We conclude that this is a radio-quiet AGN, with no evidence for a strong IR dust component.

The data shown in Fig. 7 suggest that the optical continuum may be dominated by an extrapolation of the X-ray power law, and that the BBB and the soft X-ray excess are relatively weak. The optical spectrum shows no features typical of significant emission from the host galaxy (see Fig. 1). The apparent turn-up towards the blue shortward of 4000 Å may be the so-called 'little' blue bump (Wills, Netzer & Wills 1985), a false excess continuum caused by the combination of a strong Balmer continuum and Fe II blends. Such a feature would not be unexpected in RX J1042 + 1212, given the strength of the Balmer *lines* and Fe II lines at other wavelengths.

In most radio-quiet AGN, the BBB dominates the energy output of the source. When this component is strong, the optical slope (α_{opt}) is very hard (i.e., it rises strongly towards the blue) and the optical to X-ray ratio (α_{ox}) is high. For example, in samples of optically selected AGN (such samples preferentially select objects with strong BBBs), the median α_{opt} is $\sim$0.2–0.3 (e.g. Neugebauer et al. 1987; Francis et al. 1991), while in the Wilkes et al. (1994) sample of PG quasars, the mean $\alpha_{ox} = 1.50$. In contrast, the RIXOS AGN sample, which is X-ray-selected, has a softer mean α_{opt} (0.9) and a lower mean α_{ox} (1.1), i.e., the 'mean' optical to X-ray continuum has no significant BBB component and a spectral index $\alpha \sim 1$. The α_{opt} and α_{ox} for RX J1042 + 1212 are both typical of the means of the RIXOS AGN [i.e., for RX J1042 + 1212, $\alpha_{opt} = 1.0 \pm 0.5$ (P96) and $\alpha_{ox} = 1.20 \pm 0.14$]; thus we find that the BBB is probably intrinsically weak in this source.

None the less, we have no data in the UV or the EUV where the peak of the BBB generally lies, and it is possible

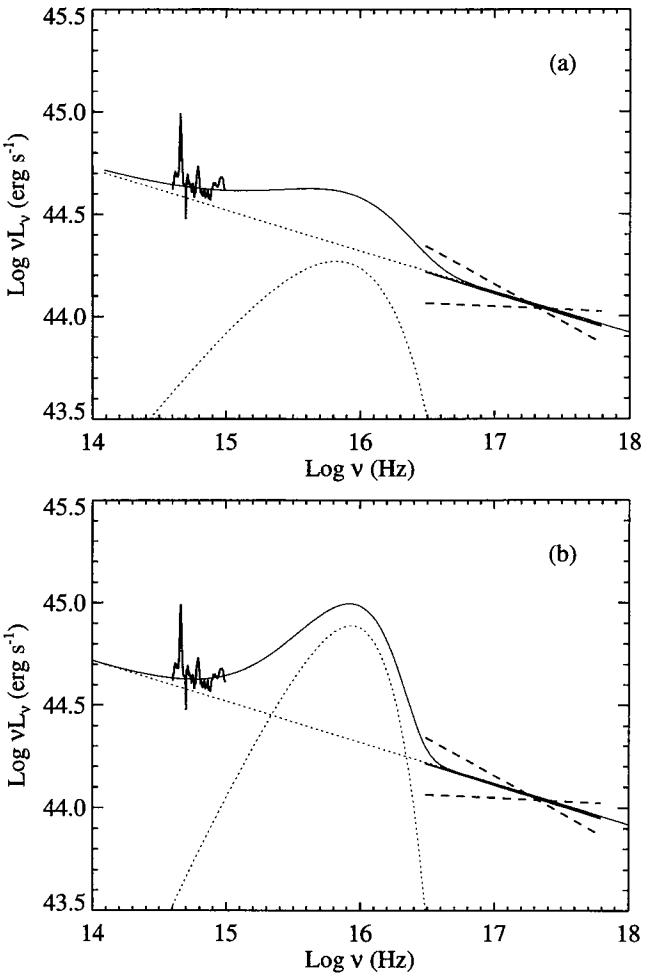

Figure 7. The optical and X-ray spectra of RX J1042 + 1212 are compared here with two different models for the optical to X-ray continuum. In (a), the BBB is modelled using a bremsstrahlung spectrum with $T_{brem} = 4 \times 10^5$ K, while in (b), a simple AD model with $T = 25$ eV has been assumed. In both cases there is an underlying $\alpha = 1.2$ power law and different thermal models have been added to assess an upper limit on the strength of the BBB. The sum of the thermal and non-thermal spectra are plotted as solid lines and individual components as dotted lines.

that the BBB may emerge significantly above the underlying continuum out of our observed range. We have therefore estimated the upper limit on the strength of a possible thermal UV component by comparing RX J1042 + 1212 with two different models of the BBB and using the optical and X-ray data as constraints at low and high energies. A thermal bremsstrahlung spectrum and a simple AD model (Pringle 1981) were used to represent the BBB (Figs 7a and b respectively), while in each case the best-fitting power-law model to the X-ray data (model 2 in Table 2; $\alpha_x = 1.2$) was used for the underlying non-thermal continuum. The bremsstrahlung spectrum has a temperature, $T_{brem} = 4 \times 10^5$ K (in the AGN rest-frame) and a total luminosity of 6×10^{44} erg s^{-1} (all luminosities have been calculated assuming a value of 50 km s^{-1} Mpc^{-1} for the Hubble constant, H_0, and 0 for the deceleration parameter, q_0). The AD has a maximum temperature of 25 eV, a luminosity of 1.5×10^{45} erg s^{-1}, and the mass of the black hole is 4×10^6 $M_\odot$. The luminosity in the power law from $\log \nu = 14$ to 18 (ν in Hz) is 2.1×10^{45} erg s^{-1}.

By integrating these models over $\log \nu = 14$ to 18, we measure total luminosities of $L_{opt,X\text{-}ray} = 3 \times 10^{45}$ and 4×10^{45} erg s^{-1} for the bremsstrahlung and AD models respectively. If we assume that this part of the spectrum dominates the bolometric luminosity, L_{bol} (since RX J1042 + 1212 is not detected longwards of 10 μm), this would imply a mass for the central black hole of at least $\sim 2 \times 10^7$ $M_\odot$ (from the Eddington limit); for the AD model this in turn suggests that the system would be super-Eddington, i.e., $L \sim 10 L_{Edd}$ (and thus the thin-disc approximation we have used is not self-consistent).

3.3 Further comparisons with other AGN

3.3.1 Balmer line properties

The mean Hα FWHM for the RIXOS AGN is 2300 ± 2200 km s^{-1} (1σ standard deviation); thus in RX J1042 + 1212, where the FWHM are ~10 000 km s^{-1} (see Tables 3 and 4), the Balmer lines are very broad for an X-ray-selected object. They are also broad when compared to optically selected quasars, e.g., for the Boroson & Green (1992, hereafter BG) sample, we calculate a mean Hβ FWHM of 3800 ± 2100 km s^{-1} (1σ). They are closer to the range for the 'disc-like' emitters from the Eracleous & Halpern (1994) sample of radio galaxies and radio-loud quasars. These are objects whose Balmer line profiles are double-peaked and are well fitted by an AD model; they have a mean Hα FWHM of 12 500 ± 4900 km s^{-1} (1σ) and range of 6800 to 23 200 km s^{-1}.

The EWs of the Balmer lines in RX J1042 + 1212 are both high relative to the means for the RIXOS sample, which has means of 100 and 40 Å for Hα and Hβ respectively. However, the ratios of the Balmer line luminosities to the X-ray luminosity ($L_{2\,keV}$) *are* typical of other objects in the RIXOS sample, suggesting that the lines are merely responding to an enhanced ionizing continuum.

3.3.2 [O III]

The EW of [O III] λ5007 is ~6 Å, which is weak relative to the means for the RIXOS sample (30 Å), the Stephens sample (44 Å) and the BG sample (24 Å). However, the logarithm of the [O III] λ5007 luminosity (41.5 erg s^{-1}) is similar to the means that we calculate for the RIXOS and Stephens (1989) samples (41.7 ± 0.6 and 41.9 ± 0.6 erg s^{-1} respectively), suggesting that it is a high optical continuum which causes the low EW, rather than intrinsically weak line emission. This may be due to variability, e.g., if the nuclear spectrum has strengthened recently so that the narrow-line region has not yet had time to respond.

3.3.3 Optical and X-ray continua

We find that the log of the continuum luminosity at 5000 Å, $L_{5000} = 29.7 \pm 0.3$ erg s^{-1}, is somewhat high compared to the RIXOS AGN where the mean $L_{5000} = 29.2 \pm 0.5$ erg s^{-1} (1σ standard deviation; this mean has been calculated only for those sources whose z is low enough to permit the detection of Hβ, i.e., at $z < 0.95$). However, if we compare the

4.1.3 *Double jets or cones*

In the jet model (e.g. Foltz, Wilkes & Peterson 1983; Zheng et al. 1990, 1991), material moving radially outwards is illuminated in a double-cone geometry. The material itself may be emitted in a double-cone, or material moving out (e.g., spherically) may be lit up by a cone-shaped or otherwise anisotropic radiation pattern. This model has many free parameters, providing the flexibility to fit many different profile shapes and variability patterns (Zheng et al. 1990). Zheng et al. (1991) fitted a double-stream model to the Hα profile of 3C 390.3, consisting of a broad component with an opening angle of 60° and a narrower component with an opening angle of 25°; the latter contributed 20 per cent of the total Hα emission. The broad component produces a flat profile, while the peaks are emitted by the narrow component.

The second fit to the Hα profile of RX J1042 + 1212 [model (2) in Table 3] suggests a crude analogy with this model, where the peaks are superimposed on one broad underlying component. It is also possible that only the peaks are produced in jets, whereas the broad underlying component is emitted from a more typical BLR (which is thought to be disc-shaped for the low-ionization lines; e.g. Krolik et al. 1991; O'Brien, Goad & Gondhalekar 1994). However, the peaks in RX J1042 + 1212 have smaller velocities than those inferred for 3C 390.3, suggesting that for RX J1042 + 1212 perhaps (1) the jets extend to larger distances, (2) the jets are viewed at a greater angle to the line of sight, or (3) the net velocity of the material in the jets of RX J1042 + 1212 is small. Note that for case (2), however, if a dusty, molecular torus lies beyond the BLR of RX J1042 + 1212 (see, e.g., Antonucci 1993, and references therein), then this will occult much of the receding jet when the system is viewed at large angles to the line of sight (assuming that the torus and jet axes are coaligned) so that the red peak would be very weak.

In Section 3.2, we showed that the data imply an enhanced power-law component common to the optical and X-ray ranges. We can speculate that this may be related to a double-sided jet, i.e., perhaps the jet was formed during an outburst or a high state of non-thermal activity. The extra ionizing continuum might also power the very broad Balmer line emission (in the 'normal' high-velocity BLR). This concept would provide a link between an enhanced very broad-line flux, double peaks and a strong non-thermal continuum. It is similar to an idea previously suggested for NGC 1097 by Storchi-Bergmann et al. (1993), i.e., that the recent appearance of double-peaked Balmer emission in this source was due to the formation of a new optical jet.

With so many free parameters for the jet model (e.g., the opening angle of the cone, inner and outer extents of the line-emitting portion, line emissivity and velocity laws throughout the cone, etc.; these may also be independent parameters for the separate red and blue cones), constraints from the present RX J1042 + 1212 data are hard to find. If changes in the line emission from the jets are induced by the central ionizing source, then the response in the red component should lag the blue (and probably by several years; Livio & Pringle 1996); thus variability studies may provide an observational test of this model. For the present, however, we find that the RX J1042 + 1212 data are consistent with a double-sided jet model for the BLR.

4.2 Double-peaked lines in radio-quiet AGN

The rarity of double-peaked lines amongst radio-quiet objects seems puzzling. Eracleous & Halpern (1994) proposed that ADs in radio-quiet AGN are intrinsically different due to different accretion rates and the availability of fuel. They suggested that an ion torus forms in the centre of radio-loud objects because the accretion rate is very low (this idea was originally proposed by Rees et al. 1982). The ion torus collimates the radio jets and provides a source of illumination for the outer edges of the AD, producing double-peaked emission lines. In radio-quiet AGN, the accretion rates are generally higher so that the ion torus, and thus also the radio jets and the double-peaked lines, would not form.

We have found that an AD is unlikely to be the source of the double-peaked lines in RX J1042 + 1212, and similar conclusions have been reached for three other double-peaked radio-quiet Seyferts (Marziani et al. 1992; Bower et al. 1996). So perhaps the source of the double-peaked emission in radio-quiet AGN is physically different from that in radio-loud objects, i.e., if the AD model is (in most cases at least) appropriate for radio-loud AGN, then a binary BLR or double-jet may be more likely for radio-quiet objects. This in turn implies that supermassive binaries (where the black hole masses are similar in size and nature) and bipolar line-emitting jets are both very rare.

The binary BLR and bipolar jet models are also viable candidates for radio-loud, double-peaked AGN (as well as radio-quiet); why should these prefer a radio-loud host? One obvious physical link between the supermassive binary and radio-loud AGN models is that both are expected to have low accretion rates (Begelman et al. 1980; Rees et al. 1982). In the bipolar jet model, the presence of a biconical, outflowing BLR seems natural in an environment which must already be dominated by the outflows of the radio jets.

5 CONCLUSIONS

RX J1042 + 1212 is an X-ray-selected AGN whose Hα and Hβ emission lines exhibit double-peaked profiles. The 'blue' peak has a velocity of -1600 km s^{-1} relative to the systemic velocity, and the 'red' peak has a relative velocity of 1000 km s^{-1}. Using combinations of Gaussians, we show that the Hα profile may be modelled as (1) two narrow peaks superimposed on one broad underlying feature, or (2) as a pair of lines each composed of a broad and a narrow component, with the central wavelength of the broad component fixed to that of its associated narrow line.

The *ROSAT* PSPC spectrum is well fitted by a power law with an energy spectral index $\alpha_x = 1.2 \pm 0.2$, and shows no evidence for significant soft X-ray absorption by cold gas or a strong soft X-ray excess. The optical continuum has a similar slope ($\alpha_{opt} = 1.0 \pm 0.5$), with little evidence for a strong BBB, except perhaps at the blue extreme of the spectrum (i.e., at rest wavelengths below ~ 4000 Å, although this may be the 'little' blue bump, a false continuum made of Balmer continuum emission and blends of

(Gaskell 1983); the existence of supermassive binaries was first discussed in detail by Begelman et al. (1980). In this model, the BLRs are gravitationally bound to their respective black holes, which are in orbit around each other, so that the line profiles for each BLR are separated and displaced from the centre. It has also been suggested that even separate orbiting *narrow*-line regions (NLRs) exist in Mrk 78 and 266 (see Gaskell 1988). However, Chen et al. (1989) have argued that the line profile which would actually be observed from a binary BLR would rarely be double-peaked; the low-velocity clouds, which presumably lie at large distances, would not orbit their respective black holes but the centre of mass of the two, 'filling-in' the core of the profile. However, these clouds may have been stripped away during the formation of the binary (Begelman et al. 1980), or the cloud velocities may not be dominated by the gravitational potential (Stockton & Farnham 1991); in either case, a double-peaked profile may be observed.

While investigating their models of supermassive black hole binaries, Begelman et al. (1980) envisaged that the ratio of the black hole masses would be ~ 10. In this case, activity at the larger component is likely to dominate the system, so that just a single displaced emission line would be observed. However, it is possible that two similar, independent nuclei may form the binary, and this was in fact suggested for OX 169 by Stockton & Farnham (1991) and may also be true of RX J1042 + 1212, given that the Balmer line profiles are similar for these two AGN.

A measurement of the ratio of the black hole masses in a supermassive binary may be derived from the relative velocities of the red and blue peaks. The blue peak in RX J1042 + 1212 has a velocity of -1600 km s^{-1} relative to the systemic velocity (assuming that this is defined by the redshift of [O III] λ5007), and the red peak has a relative velocity of 1000 km s^{-1}. This gives a mass ratio of 1.6, which is similar to that derived for OX 169 (2.9; Stockton & Farnham 1991). A lower limit for the total mass of the black holes may be calculated using the Eddington limit. We estimate a bolometric luminosity, $L_{\rm bol}$ of $\sim 4 \times 10^{45}$ erg s^{-1} from the optical to X-ray fits shown in Fig. 7, which in turn implies a black hole mass, $M > 2 \times 10^7$ M$_\odot$.

The model for the Hα profile shown in Fig. 4(b) uses a single, broad underlying Gaussian plus two narrower peaks. Taken literally, this would suggest the presence of one very broad-line region and two distinct 'intermediate'-line regions, which is clearly inconsistent with the binary BLR model. A more appropriate model would have two high- and two low-velocity regions of the BLR, so we have tested this by fitting four such Gaussians to the Hα profile. The positions of each of the Gaussian pairs were fixed at those for the red and blue peaks in model (2) for Hα, i.e., at 6526 and 6583 Å, and all other parameters were free. The best fit is shown in Fig. 8, and compares well with the data. The FWHM of the broad red and blue components are 12200 and 8600 km s^{-1} respectively, and their flux ratio is 1.5. The FWHM of the narrow components are 1500 and 1400 km s^{-1} for the red and blue components respectively, while their flux ratio is 1.8, i.e., similar to that for the broad components.

During the longest evolutionary phase of a supermassive binary, the system will be in a quiescent state and the black hole separation is almost constant. However, if the source undergoes some fuelling during this state, it will become a strong non-thermal emitter (Begelman et al. 1980). In Section 3.2, we showed that the optical to X-ray continuum of RX J1042 + 1212 appears to be dominated by a non-thermal component; thus this AGN may contain a supermassive binary which is in a 'high state', i.e., in a fuelling phase. In a system where one of the components dominates, this activity would be concentrated at the larger hole. In RX J1042 + 1212, the Hα peak displacements suggest that the components are similar in size, so perhaps the activity is more evenly divided, producing the observed line emission. If low-velocity gas has been ejected by the binary, then the profiles may well have the double-peaked profiles observed. Meanwhile, each very broad-line region would see an additional ionizing continuum, perhaps illuminating regions which would otherwise be in shadow and producing the strong, broad Balmer lines.

We conclude that the data presented here are consistent with the binary black hole model for the double-peaked emission, although more data would be required for a thorough evaluation; for example, long-time-scale variability studies could be used to search for evidence of shifts in the positions of the peaks. The orbital period of the binary may be estimated using the relationship $P = 550\, R_{18}^{3/2}\, M_9^{-1/2}$ yr (from Kepler's third law; Halpern & Filippenko 1988), where R_{18} is the distance between the two components in units of 10^{18} cm, and M_9 is the sum of the black hole masses in units of 10^9 M$_\odot$. Assuming that the binary separation is 1 pc (which is roughly the distance to the outermost regions of the BLR in Seyfert galaxies) and that the sum of the black hole masses is 10^8 M$_\odot$ (i.e., from the Eddington limit, assuming that the system is radiating at $0.2 L_{\rm Edd}$; see Section 3.2), this gives an orbital period of about 1000 yr. Thus we would not expect to see any changes in the peaks' positions over many years. Alternatively, imaging data might reveal evidence of galaxy mergers, such as regions of enhanced star formation, like that seen in OX 169 (Stockton & Farnham 1991), bridges and tails.

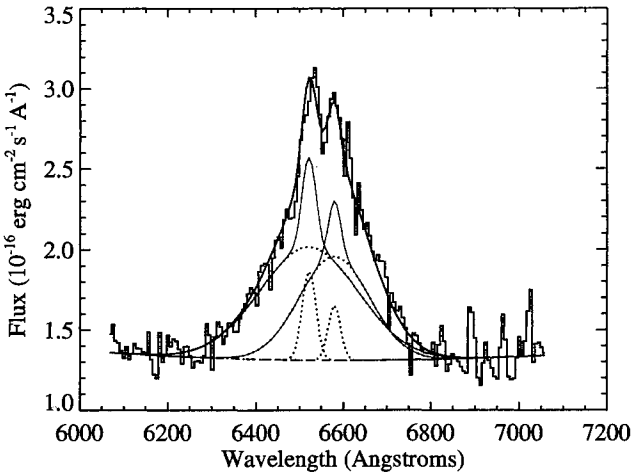

Figure 8. The Hα profile compared with a four-Gaussian component fit. The total fit is plotted as a thick solid line, the continuum as a dashed line and individual Gaussians (plus the continuum) as dotted lines. The 'pair' of profiles implied by the fits is plotted with thin, solid lines.

absolute V magnitude of RX J1042+1212 ($M_V = -22.4$) with that of the BG UV-excess quasars, we find that it is relatively weak in the optical (we calculate a mean M_V for the BG objects of -24.2 ± 1.5), yet the lines in RX J1042+1212 are broader and double-peaked. Apparently, it is not simply the strength of the optical continuum which forms these Balmer lines.

The optical to X-ray continuum in RX J1042+1212 seems to be remarkably flat overall (i.e., $\alpha_{opt} = 1.0 \pm 0.5$, $\alpha_{ox} = 1.2 \pm 0.1$ and $\alpha_x = 1.2 \pm 0.2$), suggesting that a non-thermal component dominates throughout. It is possible then that the presence of a strong power-law spectrum is related to the production of the broad, double-peaked lines. We have thus searched the RIXOS AGN for objects with similar spectra, i.e., those whose α_x, α_{opt} and α_{ox} were between 0.5 and 1.5, whose L_{5000} was greater than 29.5 erg s^{-1} and whose optical spectrum covered the Hβ region. There are two AGN (in addition to RX J1042+1212) which meet these criteria, namely source 301 in field 232 (F232-301) and source 30 in field 211 (F211-030). However, F215-019 and F232-301 have Hβ FWHM of only 1000 and 2600 km s^{-1} respectively; thus it is unlikely that the line profiles in RX J1042+1212 are solely due to a strong non-thermal component.

3.4 Summary

We find that the Hα and Hβ line emission in RX J1042+1212 is very broad and double-peaked. The BBB is relatively weak and the optical to X-ray continuum may be dominated by a non-thermal component with a slope, $\alpha \sim 1.2$. This source was not detected at radio or IR wavelengths.

The double-peaked line emission cannot be exclusively related to the shape and/or the strength of the ionizing continuum, since there are examples of AGN which do not have broad or double-peaked line profiles, yet have optical to X-ray continua which are otherwise similar in nature. This implies that there may be some phenomenological difference in RX J1042+1212 which has (as yet) only manifested itself in the Balmer line emission, although it may have some connection with the strong non-thermal component.

4 DISCUSSION

The discovery of broad, double-peaked Balmer emission in RX J1042+1212 is intriguing. The double peaks indicate that, for the low-velocity, broad-line-emitting gas at least, there are two distinct components, one moving towards us and the other moving away (relative to the systemic velocity; this may also be true of the high-velocity gas). Yet double-peaked line emission is an unusual property of AGN in general, and it is found mostly in *radio-loud* objects (see Eracleous & Halpern 1994, and references therein), even though these are outnumbered by their radio-quiet counterparts in the general AGN population by ~ 10 to one. As a *radio-quiet* double-peaked AGN RX J1042+1212 is thus extremely rare [other examples are NGC 5548 (Peterson, Korista & Cota 1987), Akn 120 (Peterson et al. 1983; Marziani, Calvani & Sulentic 1992) and IC 4329A (Marziani et al. 1992)], which adds to its already strange nature.

In this section, we discuss models of double-peaked line profiles to establish whether they can also predict other properties of RX J1042+1212, such as the strong high-velocity BLR and the dominating power law.

4.1 Models for double-peaked emission

4.1.1 Accretion discs

Optically thick accretion discs (ADs) are often invoked to explain the origin of the BBB in AGN (e.g. Shakura & Sunyaev 1973; Czerny & Elvis 1987; Madau 1988; Sun & Malkan 1989), and it has also been suggested that conditions at the outer edges of an AD may be suitable for the production of the low-ionization lines (which include Hα and Hβ; Collin-Souffrin et al. 1980; Collin-Souffrin 1987). The presence of an additional photoionizing source, e.g., by a non-thermal source, a hot corona or an ion torus (Rees et al. 1982), is required to power the line emission, as the gravitational energy available in the disc is barely sufficient on its own (e.g. Dumont & Collin-Souffrin 1990; Marziani et al. 1992). The profiles of lines from an AD are expected to be double-peaked (e.g. Chen, Halpern & Filippenko 1989; Fabian et al. 1989; Dumont & Collin-Souffrin 1990), and AD models have been successfully used to predict the Balmer lines of several AGN. For example, Eracleous & Halpern (1994) surveyed the Hα emission of 94 radio galaxies and radio-loud quasars, and identified 12 objects whose line profiles were well fitted by an AD. Other studies of individual objects include those of Pérez et al. (1988; 3C 390.3), Alloin et al. (1988; Akn 120) and Rodriguez-Ardila et al. (1996; C16.16). ADs have also been invoked to explain the skewed Fe Kα line observed in the *ASCA* spectrum of the Seyfert 1 galaxy MCG-6-30-15 (Tanaka et al. 1995).

AD models make certain predictions about the shape of the emission lines. The blue peak will always be stronger than the red peak, due to relativistic beaming, and the entire line will have a net gravitational redshift (e.g. Chen & Halpern 1989). Yet in about one-quarter of double-peaked objects, the red peak is stronger than the blue (e.g., PKS 1020−103; Eracleous & Halpern 1994), while in 3C 390.3 for example, the Hα profile is variable and has been observed to change from blue-dominant to red-dominant (Zheng et al. 1991), contradicting AD models. Some of these problems have been overcome by Eracleous et al. (1995), who invoked elliptical discs, formed by the tidal perturbation of a binary black hole or from the debris of a tidally disrupted star.

In the case of RX J1042+1212, we find that the blue peak of Hα is slightly stronger than the red (Fig. 4 and Table 3), but there is no evidence for any net gravitational redshift of the line; the central wavelength of the single component fit lies at 6553 Å, which would rather imply a net *blueshift* equivalent to a velocity of ~ 500 km s^{-1}. This is inconsistent with the AD model which, even in the elliptical case, predicts that the line will always have a net redshift (Eracleous & Halpern 1994). Thus we conclude that an AD is unlikely to be the origin of the Balmer lines in RX J1042+1212.

4.1.2 A binary BLR

One alternative to the AD model is that of two separate BLRs orbiting a supermassive black hole binary system

Fe II). It is consistent with an extrapolation of the X-ray power law, and suggests that the optical to X-ray continuum may be dominated by a non-thermal component. We estimate that any possible thermal component contributes at most ~40 per cent of the total luminosity between $\log \nu = 14$ and 18 (ν in Hz).

We have compared these results with three different models of the double-peaked profiles, an AD, a binary BLR and a double-cone geometry of the BLR. Both Hα and Hβ show a net blueshift with respect to the [O III] $\lambda\lambda$4959, 5007 lines; thus we find that AD models of the Balmer line emission, which predict a net gravitational redshift, are not appropriate for this object. The binary BLR model predicts that the two black holes must be similar in size and nature. The system would probably be in a 'high' state, i.e., accreting gas at an unusually high rate, which may produce the strong non-thermal component which is observed. The double-jet model is also possible; the data imply that the velocity in the jets must be quite low, which might be because the velocity is intrinsically low, because of orientation effects or flows which reach to relatively large distances.

ACKNOWLEDGMENTS

We are very grateful to Jim Condon for providing the VLA Sky Survey data. The optical spectrum was provided by the RIXOS consortium, and we thank all those who have contributed to the RIXOS project. This researcli has made use of LEDAS, the Leicester Database and Archive Service.

REFERENCES

Alloin D., Boisson C., Pelat D., 1988, A&A, 200, 17
Antonucci R., 1993, ARA&A, 31, 473
Begelman M. C., Blandford R. D., Rees M. J., 1980, Nat, 287, 307
Boroson T. A., Green R. F., 1992, ApJ, 80, 109 (BG)
Bower G. A., Wilson A. S., Heckman T. M., Richstone D. O., 1996, AJ, 111, 1901
Chen K., Halpern J. P., 1989, ApJ, 344, 115
Chen K., Halpern J. P., Filippenko A. V., 1989, ApJ, 339, 742
Collin-Souffrin S., 1987, A&A, 179, 60
Collin-Souffrin S., Dumont S., Heidemann N., Joly M., 1980, A&A, 83, 90
Czerny B., Elvis M., 1987, ApJ, 321, 305
Dumont A. M., Collin-Souffrin S., 1990, A&AS, 83, 71
Edelson R. A., Malkan M. A., 1986, ApJ, 308, 509
Elvis M. et al., 1994, ApJS, 95, 1
Eracleous M., Halpern J. P., 1994, ApJS, 90, 1
Eracleous M., Livio M., Halpern J. P., Storchi-Bergmann T., 1995, ApJ, 438, 610
Fabian A. C., Rees M. J., Stella L., White N. E., 1989, MNRAS, 238, 729
Foltz C. B., Wilkes B. J., Peterson B. M., 1983, AJ, 88, 1702
Francis P. J., Hewett P. C., Foltz C. B., Chaffee F. H., Weymann R. J., Morris S. L., 1991, ApJ, 373, 465
Gaskell C. M., 1983, Liège Astrophysical Colloquium, 24, 473
Gaskell C. M., 1988, in Miller R. H., Wiita P. J., eds, Active Galactic Nuclei. Springer-Verlag, Berlin, p. 61
Halpern J. P., Filippenko A. V., 1988, Nat, 331, 46
Horne K., 1986, PASP, 98, 609
Krolik J. H., Horne K., Kallman T. R., Malkan M. A., Edelson R. A., Kriss G. A., 1991, ApJ, 371, 541
Livio M., Pringle J. E., 1996, MNRAS, 278, 35
Madau P., 1988, ApJ, 327, 116
Marziani P., Calvani M., Sulentic J. W., 1992, ApJ, 393, 658
Mukai K., 1990, PASP, 102, 212
Neugebauer G., Green R. F., Matthews K., Schmidt M., Soifer B. T., Bennet J., 1987, ApJS, 63, 615
O'Brien P. T., Goad M. R., Gondhalekar P. M., 1994, MNRAS, 268, 845
Pérez E., Penston M. V., Tadhunter C., Mediavilla E., Moles M., 1988, MNRAS, 230, 353
Peterson B. M., Foltz C. B., Miller H. R., Wagner R. M., Crenshaw D. M., Meyers K. A., Byard P. L., 1983, AJ, 88, 926
Peterson B. M., Korista K. T., Cota S. A., 1987, ApJ, 312, L1
Peterson B. M., Korista K. T., Wagner R. M., Reichert G. A., 1990, ApJ, 352, 68
Pfeffermann E. et al., 1986, Proc. SPIE, 733, 519
Pringle J. E., 1981, ARA&A, 19, 137
Puchnarewicz E. M. et al., 1996, MNRAS, 281, 1243 (P96)
Rees M. J., Begelman M. C., Blandford R. D., Phinney E. S., 1982, Nat, 295, 17
Rodriguez-Ardila A., Pastoriza M. G., Bica E., Maza J., 1996, ApJ, 463, 522
Shakura N. I., Sunyaev R. A., 1973, A&A, 24, 337
Stark A. A., Gammie C. F., Wilson R. F., Ball J., Linke R. A., Heiles C., Hurwitz M., 1992, ApJS, 79, 77
Stephens S. A., 1989, AJ, 97, 10
Stockton A., Farnham T., 1991, ApJ, 371, 525
Storchi-Bergmann T., Baldwin J. A., Wilson A. S., 1993, ApJ, 410, L11
Sun W.-H., Malkan M. A., 1989, ApJ, 346, 68
Tanaka Y. et al., 1995, Nat, 375, 659
Veilleux S., Zheng W., 1991, ApJ, 377, 89
Walter R., Fink H. H., 1993, A&A, 274, 105
Wilkes B., Tananbaum H., Worrall D. M., Avni Y., Oey M. S., Flanagan J., 1994, ApJS, 92, 53
Wills B. J., Netzer H., Wills D., 1985, ApJ, 288, 94
Zheng W., Binette L., Sulentic J. W., 1990, ApJ, 365, 115
Zheng W., Veilleux S., Grandi S. A., 1991, ApJ, 381, 418